Turbulence, Heat and Mass Transfer 6
K. Hanjalić, Y. Nagano and S. Jakirlić (Editors)
©2009 Begell House, Inc.

Partially Averaged Navier-Stokes Modelling of Turbulent Channel Flow with and without Forcing

J.M. Ma[1,2], L. Davidson[2], S.-H. Peng[2,3] and F.J. Wang[1]

[1]*College of Water Conservancy & Civil Engineering, China Agricultural University, Qinghua East Road 17, Haidian District, Beijing, China, jiameima@gmail.com, wangfj@cau.edu.cn*

[2]*Department of Applied Mechanics, Chalmers University of Technology, SE-412 96 Gothenburg, Sweden, lada@chalmers.se*

[3]*Department of Aeronautics and Systems Integration, Swedish Defence Research Agency (FOI), SE-16940 Stockholm, Sweden, peng@foi.se*

Abstract — Turbulent channel flow is computed using the Partially Averaged Navier-Stokes (PANS) method which is derived from a parent RANS $k-\varepsilon$ model and controlled by two parameters: the unresolved-to-total ratio of kinetic energy (f_k) and of dissipation (f_ε). Backscatter from a scale-similarity model is used as forcing which is added in the momentum equations in order to trigger resolved turbulence. A combination of the backscatter model with the PANS methodology is evaluated in channel flow. It was found that the PANS model is able to yield reasonable predictions with an appropriate value of f_k. In addition, it was demonstrated that adding forcing has the capability of creating more resolved turbulence, especially for small f_k.

1. Introduction

While Large Eddy Simulation (LES) has shown the ability to resolve flow structures and achieve more accurate predictions in which only scales larger than the grid spacing are resolved and subgrid scales are modelled [1, 2], it is often too expensive for realistic engineering applications. In the past decade, an alternative method called hybrid RANS/LES has been proposed that efficiently combines the advantages of RANS and LES approaches. A number of hybrid methods have been developed. The Detached Eddy Simulation (DES) [3] is one of the most successful hybrid methods in which the attached boundary layer is simulated using the unsteady RANS approach, while the outer flow region is computed using LES. In DES, the switch between the RANS and LES is dictated by the ratio of the RANS to the LES turbulent length scales. Another modelling method is Very Large Eddy Simulation (VLES) [4, 5] in which the very large scales of turbulence are directly calculated, and the effect of the unresolved scales is accounted for by an eddy viscosity model. However, this approach requires a substantially more sophisticated modelling approach.

Recently, the Partially Averaged Navier-Stokes (PANS) model, proposed by Girimaji [6, 7], was used with the intention to smoothly simulate turbulent flows using either of a hierarchic rank of approaches from RANS to Direct Numerical Simulation (DNS). The PANS model is derived from a parent RANS $k-\varepsilon$ model based on various modeled-to-resolved scale ratios. The PANS formulations are controlled by two parameters: the unresolved-to-total ratio of kinetic energy (f_k) and of dissipation (f_ε). One of the advantages of the PANS model is that it is easy to implement the model into an existing RANS solver. Only coefficients need to to be changed depending on the choices of f_k and f_ε [8]. The PANS model has been evaluated in

some typical turbulent separating flows. Girimaji [7] applied the PANS model to the flow past a square cylinder and the flow over a surface-mounted cube. Girimaji and Lavin [9] used the PANS model to investigate a turbulent square jet and demonstrated that PANS is capable of capturing jet physics. Basu et al. [10] applied the PANS model to a cavity with the value of f_k varying with local grid spacing and turbulent length scale. Frendi et al. [11] compared three hybrid approaches (DES, URANS and PANS), showing that the PANS model obtained better results than the other two turbulence models for a turbulent flow over a backward facing step. The influence of the PANS parameter f_ε was also investigated, and it was shown that the range of scales decreases with decreasing f_ε. It was also reported that the PANS computations are sensitive to grid resolution. Song et al. [12] focused their investigation on how to determine the control parameter f_k in the flow past a square cylinder. They proposed an equation to evaluate this parameter, and demonstrated that the PANS approach is very effective in simulating separated turbulent flows and that accurate predictions could be obtained by using a much coarser grid than is required for LES.

The present work investigates the PANS modelling for turbulent channel flow. An isotropic synthetic fluctuation is used as an inlet boundary condition for unsteady simulations [13, 14]. Backscatter from a scale-similarity model is used as forcing, in which only the part of the gradient of Reynolds stress is considered when its sign is consistent with the viscous terms [15]. In the present work, this approach is used in order to trigger resolved turbulence in simulation of attached turbulent boundary layer. If no forcing conditions are prescribed in computation, the resolved turbulence near the inlet will be too small and a large streamwise distance will be required before the modelled equations are able to re-establish fully developed turbulent flow.

The outline of the paper is as follows. We describe the scale-similarity model and the PANS formulation in section 2, and the simulation methods are presented in section 3. The results of the calculations are discussed in section 4 to demonstrate the advantages of PANS model and the effects of forcing in momentum equations. Finally, conclusions are drawn in section 5.

2. Equations

For incompressible turbulent flows, the continuity equation and Reynolds-averaged Navier-Stokes equation are given by

$$\begin{aligned} &\frac{\partial U_i}{\partial x_i} = 0 \\ &\frac{\partial U_i}{\partial t} + \frac{\partial (U_i U_j)}{\partial x_j} = -\frac{1}{\rho}\frac{\partial P}{\partial x_i} + \frac{\partial}{\partial x_j}\left[(\nu + \nu_t)\frac{\partial U_i}{\partial x_j}\right] \end{aligned} \tag{1}$$

The RANS $k-\varepsilon$ two-equation model reads:

$$\begin{aligned} &\frac{\partial k}{\partial t} + \frac{\partial (k U_j)}{\partial x_j} = \frac{\partial}{\partial x_j}\left[\left(\nu + \frac{\nu_t}{\sigma_k}\right)\frac{\partial k}{\partial x_j}\right] + P_k - \varepsilon \\ &\frac{\partial \varepsilon}{\partial t} + \frac{\partial (\varepsilon U_j)}{\partial x_j} = \frac{\partial}{\partial x_j}\left[\left(\nu + \frac{\nu_t}{\sigma_\varepsilon}\right)\frac{\partial \varepsilon}{\partial x_j}\right] + C_{\varepsilon 1} P_k \frac{\varepsilon}{k} - C_{\varepsilon 2}\frac{\varepsilon^2}{k} \\ &\nu_t = C_\mu \frac{k^2}{\varepsilon} \end{aligned} \tag{2}$$

where the production term of turbulent kinetic energy is given by

$$P_k = \nu_t \left(\frac{\partial U_i}{\partial x_j} + \frac{\partial U_j}{\partial x_i}\right)\frac{\partial U_i}{\partial x_j} \tag{3}$$

The coefficients take the values of:

$$C_{\varepsilon 1} = 1.44, C_{\varepsilon 2} = 1.92, \sigma_k = 1.0, \sigma_\varepsilon = 1.31, C_\mu = 0.09 \tag{4}$$

2.1. Scale-similarity model used as forcing

In scale-similarity model, the largest unresolved scales are assumed to be similar to the smallest resolved scales. This is the elementary idea of scale-similarity subgrid models. The dissipative part of the Reynolds stress term, $\partial\tau_{ij}/\partial x_j$, was added to the momentum equations in [16]. This idea is employed in the present work, and only the part of the Reynolds stress term that corresponds to backscatter is added to the momentum equations [15]. The SGS tensor is given by [17]

$$\tau_{ij} = \overline{\bar{u}_i \bar{u}_j} - \bar{\bar{u}}_i \, \bar{\bar{u}}_j \tag{5}$$

The equation for the resolved turbulent kinetic energy, $k = \langle u_i' u_i' \rangle / 2$, reads

$$\begin{aligned} \frac{Dk}{Dt} + \langle u_j' u_i' \rangle \frac{\partial \langle \bar{u}_i \rangle}{\partial x_j} + \frac{\partial \langle p' u_i' \rangle}{\partial x_i} + \frac{1}{2} \frac{\partial \langle u_j' u_i' u_i' \rangle}{\partial x_j} = \\ \nu \frac{\partial^2 k}{\partial x_j \partial x_j} - \underbrace{\nu \left\langle \frac{\partial u_i'}{\partial x_j} \frac{\partial u_i'}{\partial x_j} \right\rangle}_{\varepsilon} - \underbrace{\left\langle \frac{\partial \tau_{ij}}{\partial x_j} u_i' \right\rangle}_{\varepsilon_{SGS}} \end{aligned} \tag{6}$$

where $\nu(\partial^2 k/(\partial x_j \partial x_j))$ is the viscous diffusion term, ε is the viscous dissipation term, which is always positive, and ε_{SGS} is a source term arising from the SGS stress tensor, which can be positive or negative. When it is positive, forward scattering of turbulent energy takes place; when it is negative, backscattering occurs.

A sign function, M_{ij}, is defined to control the sign of ε_{SGS}. In the present investigation, only the backscatter part is included. The sign function is then defined as [15]

$$\begin{aligned} M_{ij}^B &= -\text{sign}\left(-\frac{\partial \tau_{ij}}{\partial x_j} \frac{\partial^2 \bar{u}_i}{\partial x_j \partial x_j} \right), \text{no summation on } i, j \\ \tilde{M}_{ij}^B &= \max(M_{ij}^B, 0) \\ \frac{\partial \tau_{ij}^B}{\partial x_j} &= \tilde{M}_{ij}^B \frac{\partial \tau_{ij}}{\partial x_j}, \text{no summation on } i, j \end{aligned} \tag{7}$$

where superscript B indicates backscatter. The term $-\partial\tau_{ij}^B/\partial x_j$ is added to the momentum equations.

Thus, the momentum equations with an added forcing can be written as:

$$\frac{\partial U_i}{\partial t} + \frac{\partial (U_i U_j)}{\partial x_j} = -\frac{1}{\rho} \frac{\partial P}{\partial x_i} + \frac{\partial}{\partial x_j} \left[(\nu + \nu_t) \frac{\partial U_i}{\partial x_j} \right] - \frac{\partial \tau_{ij}^B}{\partial x_j} \tag{8}$$

where the last term is the forcing term.

2.2. PANS turbulence model

The PANS model is derived from the RANS closure equations and resolves large-scale unsteady fluctuations through a partial averaging idea. The extent of the resolved part is determined by two parameters: the unresolved-to-total ratio of kinetic energy, f_k, and of dissipation, f_ε, defined

by $f_k = k_u/k$ and $f_\varepsilon = \varepsilon_u/\varepsilon$, respectively. The PANS closure equations for k_u and ε_u are given by [6, 7]

$$\begin{aligned}
&\frac{\partial k_u}{\partial t} + \frac{\partial (k_u U_j)}{\partial x_j} = \frac{\partial}{\partial x_j}\left[\left(\nu + \frac{\nu_u}{\sigma_{ku}}\right)\frac{\partial k_u}{\partial x_j}\right] + P_u - \varepsilon_u \\
&\frac{\partial \varepsilon_u}{\partial t} + \frac{\partial (\varepsilon_u U_j)}{\partial x_j} = \frac{\partial}{\partial x_j}\left[\left(\nu + \frac{\nu_u}{\sigma_{\varepsilon u}}\right)\frac{\partial \varepsilon_u}{\partial x_j}\right] + C_{\varepsilon 1}\frac{P_u \varepsilon_u}{k_u} - C^*_{\varepsilon 2}\frac{\varepsilon_u^2}{k_u} \\
&\nu_u = C_\mu \frac{k_u^2}{\varepsilon_u}
\end{aligned} \tag{9}$$

$$C^*_{\varepsilon 2} = C_{\varepsilon 1} + \frac{f_k}{f_\varepsilon}(C_{\varepsilon 2} - C_{\varepsilon 1}) \tag{10}$$

$$\begin{aligned}
&\sigma_{ku} \equiv \sigma_k \frac{f_k^2}{f_\varepsilon}, \sigma_{\varepsilon u} \equiv \sigma_\varepsilon \frac{f_k^2}{f_\varepsilon}, \\
&P_u = \nu_u \left(\frac{\partial U_i}{\partial x_j} + \frac{\partial U_j}{\partial x_i}\right)\frac{\partial U_i}{\partial x_j}
\end{aligned} \tag{11}$$

where subscript u indicates PANS statistics (i.e. partially averaged) and k_u and ε_u are unresolved kinetic energy and its dissipation rate, respectively.

The value of f_ε is taken as 1.0 and coefficients $C_{\varepsilon 1}$, $C_{\varepsilon 2}$, σ_k, σ_ε and C_μ take the same value as in the parent RANS model. Several values of f_k were used for evaluation.

3. Simulation methods

An incompressible, finite volume code was used in the computations [18]. The second-order central differencing was used for space discretization for all terms except the convection terms in the k_u and ε_u equations, for which the hybrid central/upwind scheme was employed. The Crank-Nicolson scheme was used for time discretization of all equations. The numerical procedure is based on an implicit, fractional step technique with a multigrid pressure Poisson solver [19] and a non-staggered grid arrangement.

Isotropic synthetic fluctuations were used at the inlet boundary. The inlet turbulence has integral length and time scales are related to the grid size, Δy, Δz, and the computational time step, Δt. The detailed derivation for the inlet fluctuating velocity field can be found in [13, 14]. The fluctuating velocities are superimposed on a mean streamwise velocity profile, U_{in}, with $V_{in} = W_{in} = 0$ and

$$U^+_{in} = \frac{1}{\kappa} ln(y^+) + B \tag{12}$$

where $\kappa = 0.4$ and $B = 5.2$.

Periodic boundary conditions were used on the spanwise boundaries, and wall functions based on the instantaneous log-law were used at the wall. The modelled turbulent kinetic energy and its dissipation were prescribed at the first interior nodes. Neumann boundary conditions were used at the outlet.

A $128 \times 64 \times 32$ mesh was used in the streamwise (x), wall-normal (y) and spanwise (z) directions, respectively. The size of the computational domain was $x_{max} = 51.2$, $y_{max} = 2.0$ and $z_{max} = 1.6$, and the schematic of the channel in 2D is shown in Fig. 1. Constant grid spacing was employed in all coordinate directions, and the first grid line near the wall was located at $y^+ = 62.5$ and $\Delta y = 3.125 \times 10^{-2}$. The time step was set to $\Delta t = 5.0 \times 10^{-3}$. The Reynolds number is defined as $Re_\tau = u_\tau \delta/\nu = 4000$, where δ denotes the half height of channel and u_τ denotes the wall friction velocity.

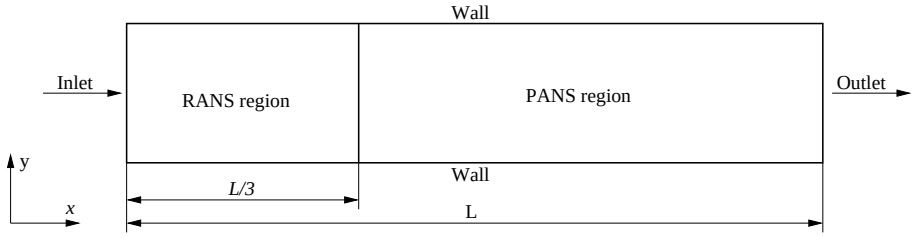

Figure 1: Schematic of channel at the $x-y$ cross-section (RANS and PANS regions)

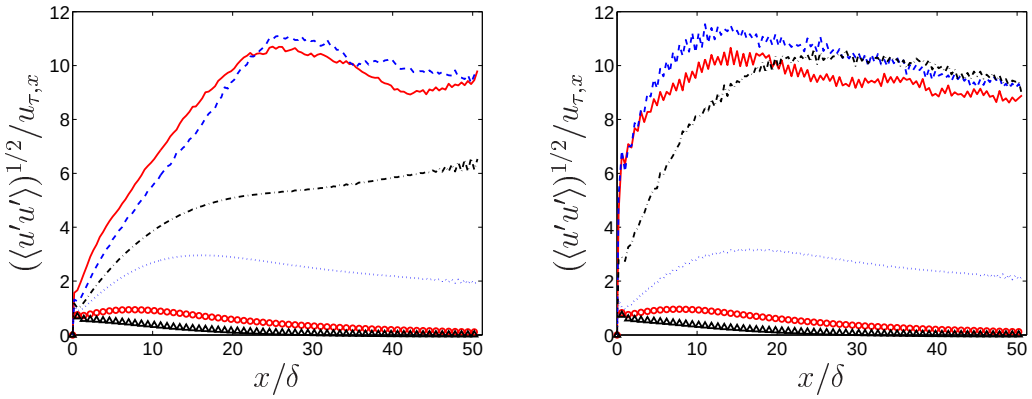

(a) WOF (b) WF

Figure 2: u_{rms} fluctuations vs. x at $y/\delta = 0.11$. —— : $f_k = 0.1$; - - - : $f_k = 0.2$; - · - : $f_k = 0.3$; ····· : $f_k = 0.4$; ○: $f_k = 0.7$; △: $f_k = 1.0$.

4. Results and discussions

The results are presented in two parts. In the first part, PANS simulations with forcing (WF) and without forcing (WOF) are presented for six constant values of f_k, namely, 0.1, 0.2, 0.3, 0.4, 0.7 and 1.0. The effect of different f_k in the PANS simulations is examined. The second part discusses computations that have been made in which one-third of the upstream channel is solved with the RANS model ($f_k = 1.0$) and PANS is used in the remaining part of the domain. In the RANS region, no forcing is added; in the PANS region, we consider the cases with and without forcing. The same group of values for f_k are used. The value of f_ε is kept as unity for all the cases.

4.1. PANS simulations with and without forcing for various f_k

The u_{rms} fluctuations are presented with and without forcing versus x for various f_k at $y/\delta = 0.11$ (see Fig. 2). As can be seen, for $f_k \leq 0.2$, the flow becomes approximately fully developed at $x/\delta = 10$ with forcing and at $x/\delta = 20$ without forcing. The fluctuations increase with decreasing f_k in both cases. The figure also shows that more turbulent fluctuations are created in the vicinity of the inlet of channel with forcing than without forcing. The $x/\delta = 45.0$ value is used in the following discussions and the quantities are compared with and without forcing of various values of f_k in this section.

The streamwise velocity profiles obtained with and without forcing are compared in Fig. 3 with the log-law. Poor behavior is observed when the value of f_k is equal to or greater than 0.4 with and without forcing, except for $f_k = 1.0$, for which the agreement with log-law is almost perfect. However, the agreement with the log-law shows a drastic improvement at $f_k = 0.3$

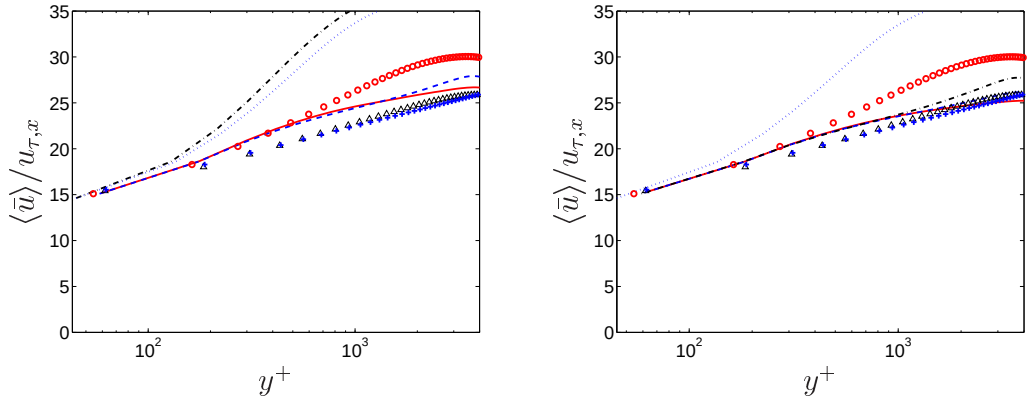

(a) WOF (b) WF

Figure 3: Velocity profiles at $x/\delta = 45.0$. —— : $f_k = 0.1$; - - - : $f_k = 0.2$; - · - : $f_k = 0.3$; ····· : $f_k = 0.4$; ○: $f_k = 0.7$; △: $f_k = 1.0$; +: $2.5ln(y^+) + 5.2$.

when forcing is added; the velocity profiles for $f_k = 0.2$ and 0.3 are very similar when no forcing is added. The figure also shows better results for $f_k = 0.1$ and 0.2 with forcing. The reason is that adding forcing generates resolved fluctuations (Fig. 2).

Figure 4 presents the modelled and resolved shear stress profiles with and without forcing for various values of f_k, and these are compared with the DNS data of $Re_\tau = 550$. With and without forcing, the modelled shear stress is reduced with a decrease in f_k. Moreover, the resolved shear stress has a strong melioration for $f_k = 0.3$ from no forcing to forcing.

Figure 5 illustrates the modeled and resolved turbulent kinetic energy, k_u, with and without forcing. As can be seen, the peak values of resolved k with forcing are larger than without forcing when f_k is smaller than 0.4. The value of the modelled k_u is compared with the result for $1D$ channel flow using the RANS model. The slight difference between the PANS with $f_k = 1.0$ and the $1D$ RANS prediction is probably due to some small unsteadiness in the resolved fluctuations by PANS.

Figure 5 also shows that the modelled turbulent kinetic energy decreases with decreasing f_k, whereas the resolved turbulent kinetic energy increases. This is observed both with and without forcing. The resolved turbulent kinetic energy is almost equal to zero for $f_k = 1.0$, as shown in Fig. 5(b) and Fig. 5(d). In this case, PANS returns to a steady RANS model. However, the resolved flow captures more and more unsteady scales of motion with decreasing f_k. The two figures also illustrate that the addition of forcing to the momentum equations plays an important role when small f_k values are invoked.

4.2. Zonal PANS simulations for various f_k

The term of zonal PANS means here that one part of the computational domain uses the RANS model and the other uses the PANS model. It is similar to a simulation using embedded LES. In the present paper, the first third of the channel is solved using the RANS model with $f_k = 1.0$, where no forcing is added to the momentum equations. In the remaining part of the channel, the PANS model is used with a lower value of f_k; the schematics are depicted in Fig.1. Two cases are considered in the PANS region, namely, with and without forcing added to the momentum equations.

Figure 6 shows the u_{rms} of the two cases versus x for various f_k at $y/\delta = 0.11$. Here it is clearly seen that forcing has a significant influence on turbulent fluctuations for small f_k values.

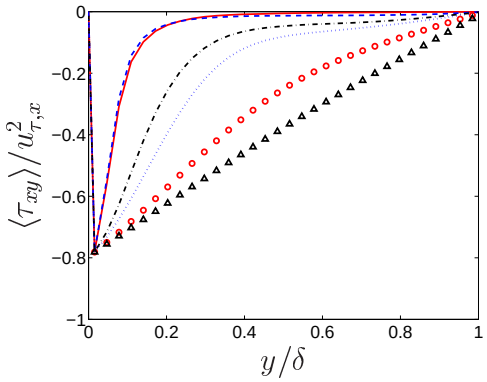

(a) Modelled shear stress, WOF

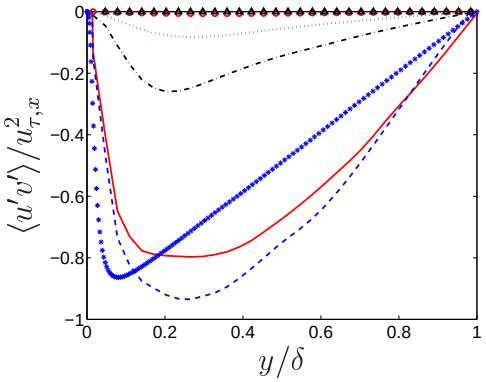

(b) Resolved shear stress, WOF

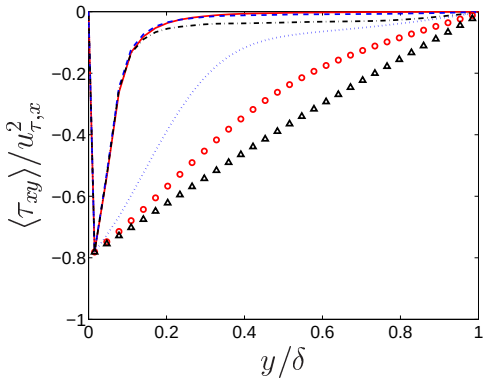

(c) Modelled shear stress, WF

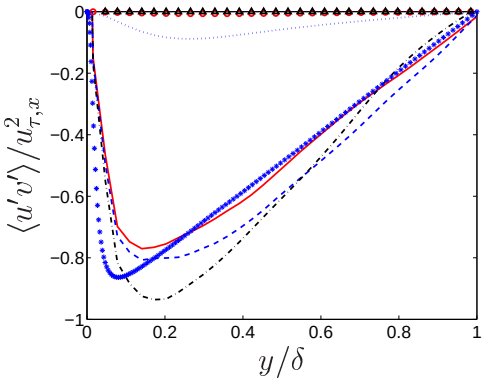

(d) Resolved shear stress, WF

Figure 4: Shear stress profiles at $x/\delta = 45.0$. —: $f_k = 0.1$; - - -: $f_k = 0.2$; - · -: $f_k = 0.3$; · · · · ·: $f_k = 0.4$; ○: $f_k = 0.7$; △: $f_k = 1.0$; ∗: DNS with $Re_\tau = 550$ [20].

A break location can be found at the interface of RANS to PANS, which lies at $x/\delta = 17.0$, see Fig. 6(b). The fluctuations rise rapidly in the RANS region and descend quickly after the interface for f_k smaller than 0.2. All simulations with the different f_k values are fully developed when approaching $x = x_{max}$ with forcing.

Turbulent viscosity versus x at $y/\delta = 0.11$ is shown in Fig. 7. It should be noted that a higher value of turbulent viscosity, ν_t, is obtained with forcing than without forcing near the interface (Fig. 7(c)). A large ν_t dampens the fluctuations, which explains why the resolved fluctuation at the exit for $f_k = 0.1$ and 0.2 is smaller with forcing than without forcing.

The location of $x/\delta = 25.0$ is considered in order to compare the quantities of the simulations. This location is 8δ downstream of the interface of the RANS to PANS models so that the influence of prediction with forcing can be observed clearly. It should be noted that the turbulence has not fully developed at this location. Although the results at $x/\delta = 45.0$ are not included, it is illustrated here that the predictions have been improved with forcing (similar to the plottings as shown in Figs. $2 - 5$). Nevertheless, the zonal PANS simulation shows better behavior for $f_k = 0.4$ with forcing than full PANS simulation, when fully developed turbulence is established.

In the RANS region, three locations have been taken to compare the influence of forcing, namely, $x/\delta = 11.0$, $x/\delta = 15.0$ and $x/\delta = 17.0$. It shows that the addition of downstream

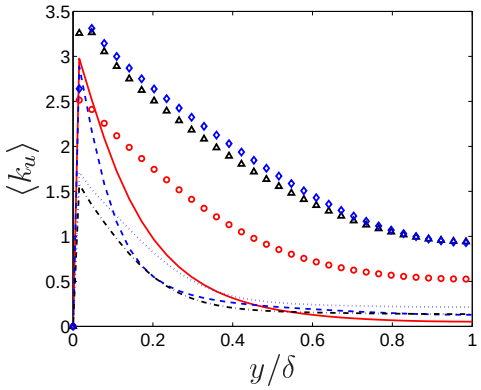

(a) Modelled k_u, WOF

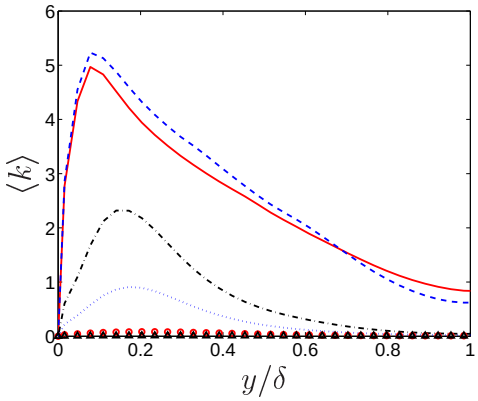

(b) Resolved k, WOF

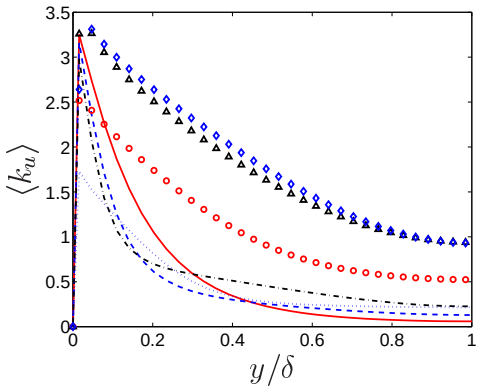

(c) Modelled k_u, WF

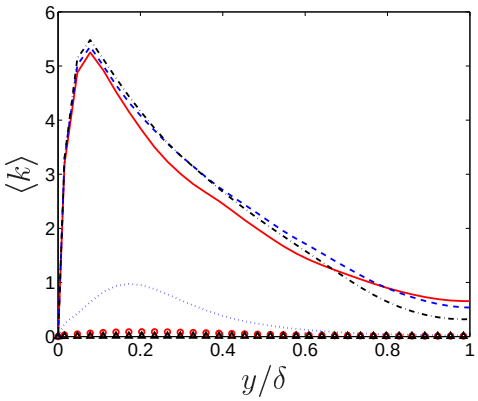

(d) Resolved k, WF

Figure 5: Turbulent kinetic energy at $x/\delta = 45.0$. —: $f_k = 0.1$; - - -: $f_k = 0.2$; - - -: $f_k = 0.3$; .....: $f_k = 0.4$; ○: $f_k = 0.7$; △: $f_k = 1.0$; ◇: from an 1D simulation with the RANS model

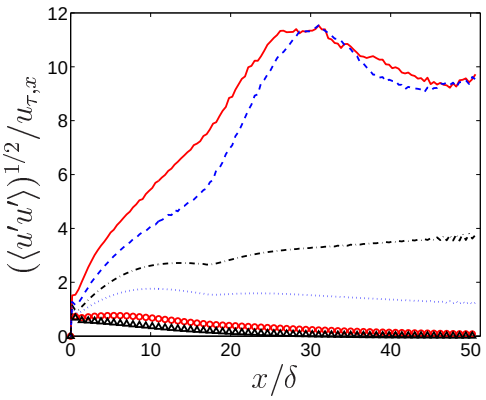

(a) WOF

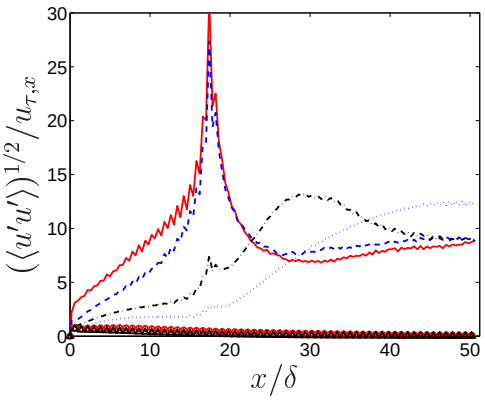

(b) WF

Figure 6: u_{rms} fluctuations vs. x at $y/\delta = 0.11$. —: $f_k = 0.1$; - - -: $f_k = 0.2$; - - -: $f_k = 0.3$; .....: $f_k = 0.4$; ○: $f_k = 0.7$; △: $f_k = 1.0$.

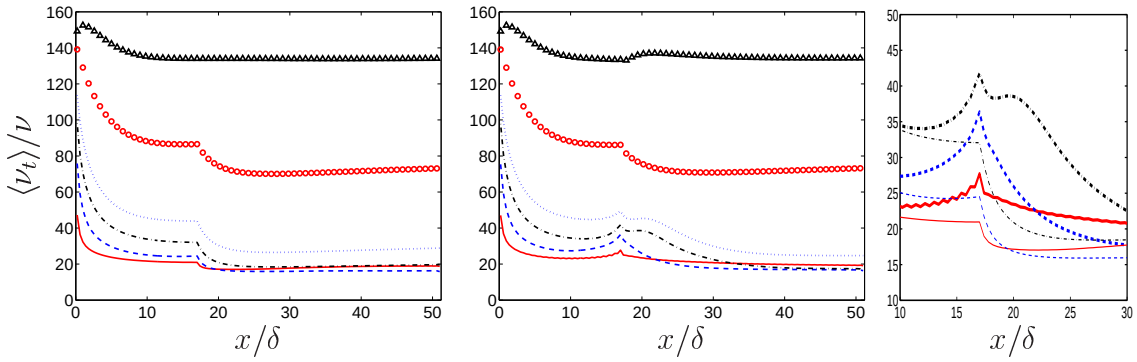

(a) WOF (b) WF (c) Zoomed view

Figure 7: Turbulent viscosity vs. x at $y/\delta = 0.11$. —: $f_k = 0.1$; - - -: $f_k = 0.2$; - - -: $f_k = 0.3$; .....: $f_k = 0.4$; ○: $f_k = 0.7$; △: $f_k = 1.0$. In the zoomed view, thick line: with forcing; thin line: without forcing.

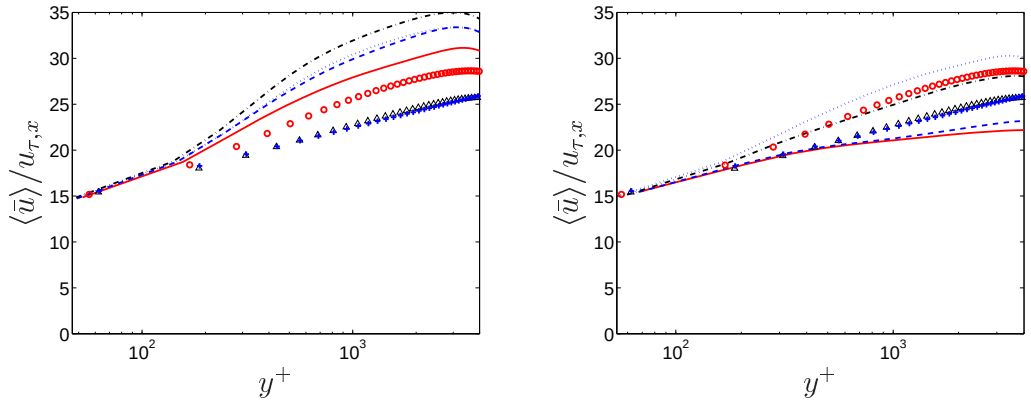

(a) WOF (b) WF

Figure 8: Velocity profiles at $x/\delta = 25.0$. —: $f_k = 0.1$; - - -: $f_k = 0.2$; - - -: $f_k = 0.3$; .....: $f_k = 0.4$; ○: $f_k = 0.7$; △: $f_k = 1.0$; +: $2.5ln(y^+) + 5.2$.

forcing has a neglectable effect in the RANS region; although the figure is not illustrated here.

The velocity profiles with and without forcing at $x/\delta = 25.0$ are compared in Fig. 8 with the log-law. As can be seen, the velocity profiles without forcing are overpredicted compared with the log-law at all values of f_k except $f_k = 1.0$, for which the agreement is almost perfect. The ratio $\langle \bar{u} \rangle / u_{\tau,x}$ is decreased for f_k smaller than 0.4 with forcing, see Fig. 8(b). This is due to the forcing, which triggers more resolved turbulence, increasing the turbulent resolved diffusion and thus decreasing $\langle \bar{u} \rangle / u_{\tau,x}$.

Turbulent viscosity with and without forcing at $x/\delta = 25.0$ is displayed in Fig. 9; $1D$ results with the RANS model are included in the figure. The turbulent viscosity increase for $f_k \leq 0.4$ when the forcing was added in the PANS region, as shown in Fig. 9(b). This is consistent with the results in Fig. 10.

The modelled and resolved turbulent kinetic energy at $x/\delta = 25.0$ are presented in Fig. 10. The $1D$ result with the RANS model is also included in the figure. Comparing these figures, we can find that adding forcing in the momentum equations indeed increases the resolved turbulent kinetic energy for $f_k \leq 0.4$. As a consequence, the production of modelled turbulence is

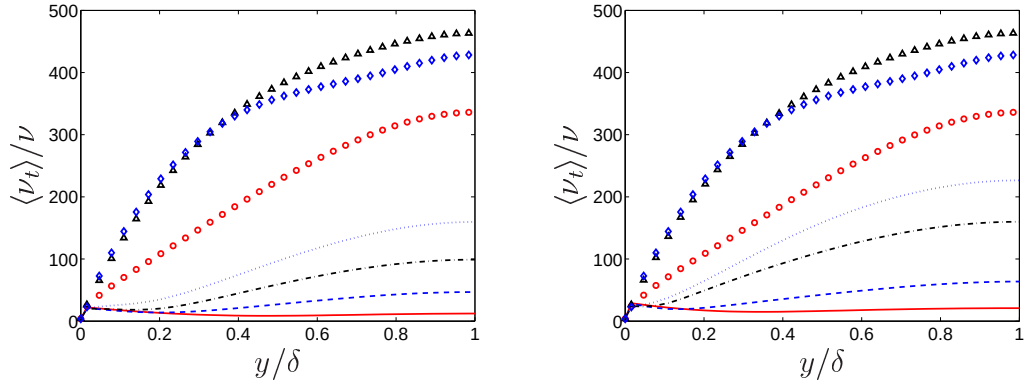

(a) WOF (b) WF

Figure 9: Turbulent viscosity at $x/\delta = 25.0$. ——: $f_k = 0.1$; - - -: $f_k = 0.2$; - - -: $f_k = 0.3$; .....: $f_k = 0.4$; ○: $f_k = 0.7$; △: $f_k = 1.0$; ◇: from an 1D simulation with the RANS model

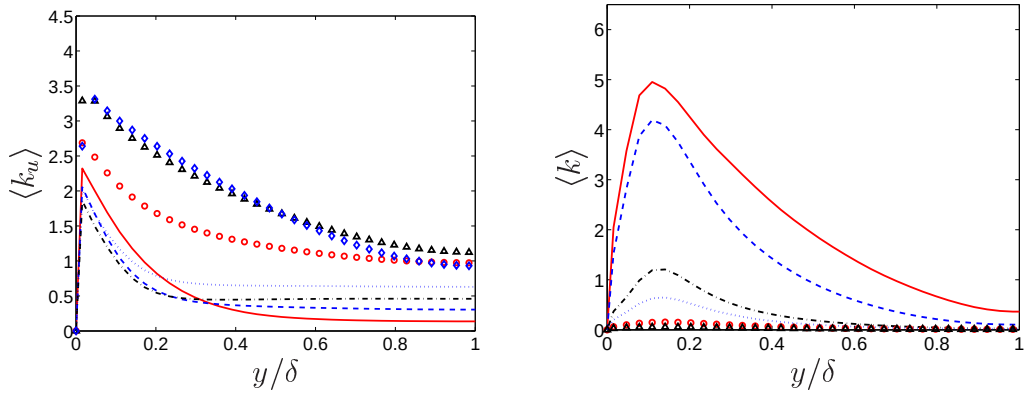

(a) Modelled k_u, WOF (b) Resolved k, WOF

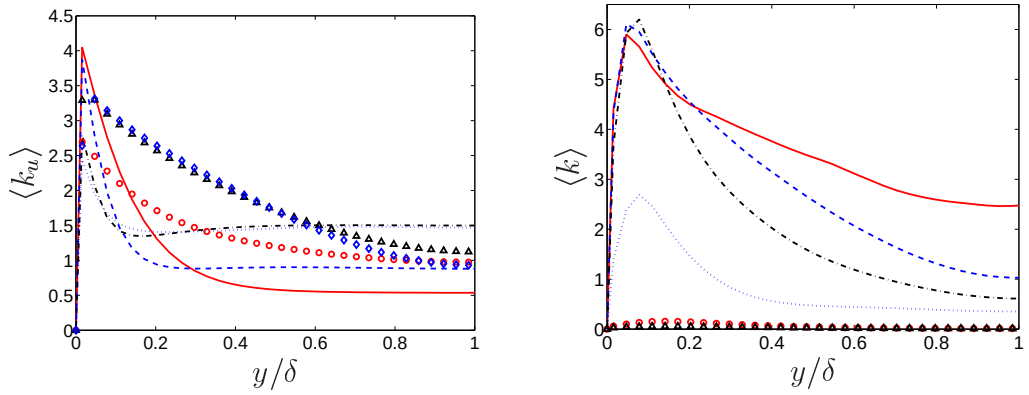

(c) Modelled k_u, WF (d) Resolved k, WF

Figure 10: Turbulent kinetic energy at $x/\delta = 25.0$. ——: $f_k = 0.1$; - - -: $f_k = 0.2$; - - -: $f_k = 0.3$; .....: $f_k = 0.4$; ○: $f_k = 0.7$; △: $f_k = 1.0$; ◇: from an 1D simulation with the RANS model

also increased. The same tendency can be observed in the results when the fully developed turbulence is re-established, for example, at $x/\delta = 45.0$.

5. Conclusions

Computations were made for turbulent channel flow using the PANS and zonal PANS models with and without forcing. The zonal PANS model means that a part (one-third in this work) of the upstream channel is solved in RANS mode ($f_k = 1.0$) and being coupled with downstream PANS with or without forcing. The forcing is represented through a scale-similarity model by including only the backscatter part.

Six constant values of f_k were used, and the influence was explored. Comparisons of the predicted results of the present PANS simulation indicate that the PANS model is able to yield reasonable predictions with an appropriate value of f_k, usually $f_k = 0.4$ or smaller. The simulations with different values of f_k clearly demonstrated that more turbulence are resolved with decreasing f_k.

Comparisons were made with and without forcing for the zonal PANS method. These clearly indicate that forcing stemming from the backscatter part of a similarity model is able to create a richer resolved turbulence. The present work has shown that the addition of forcing plays a very important role in triggering the turbulent fluctuations for small f_k values. Nevertheless, forcing does not work for large f_k values. This suggests that it is more plausible to use forcing in DNS (or LES) simulations than in RANS simulations.

6. Acknowledgments

The first author would like to acknowledge the financial support given by the China Scholarship Council, the Beijing Nature Science Foundation of China (3071002) and the National Nature Science Foundation of China (50779070). The financial support by SNIC (Swedish National Infrastructure for Computing) for computer time at C3SE (Chalmers Center for Computational Science and Engineering) is also gratefully acknowledged.

References

1. J. Smagorinsky. General circulation experiments with the primitive equations. *Monthly Weather Review*, 91:99–165, 1963.
2. M. Germano, U. Piomelli, P. Moin, and W.H. Cabot. A dynamic subgrid-scale eddy viscosity model. *Physics of Fluids A*, 3:1760–1765, 1991.
3. P.R. Spalart, W.-H. Jou, M. Strelets, and S.R. Allmaras. Comments on the feasability of LES for wings and on a hybrid RANS/LES approach. In C. Liu and Z. Liu, editors, *Advances in LES/DNS, First Int. conf. on DNS/LES*, Louisiana Tech University, 1997. Greyden Press.
4. C.G. Speziale. Turbulence modeling for time-dependent RANS and VLES: A review. *AIAA Journal*, 36:173–184, 1998.
5. N.-S. Liu and T.-H. Shih. Turbulence modeling for Very Large-Eddy Simulation. *AIAA Journal*, 44(4):687697, 2006.
6. S.S. Girimaji. Partially-Averaged Navier-Stokes model for turbulence: Implementation and Validation. In *43rd AIAA Aerospace Sciences Meeting and Exhibt*, 10-13 January, Reno, Nevada, 2005.
7. S.S. Girimaji. Partially-Averaged Navier-Stokes model for turbulence: A Reynolds-averaged Navier-Stokes to direct numerical simulation bridging method. *Journal of Fluids Engineering*, 73(2):413–421, 2006.
8. J. Fröhlich and D. von Terzi. Hybrid LES/RANS methods for the simulation of turbulent flows. *Progress in Aerospace Sciences*, 44:349–377, 2008.

9. S. S. Girimaji and T. A. Lavin. Investigation of turbulent square jet using PANS method. In M. Napolitano and F. Sabetta, editors, *44th AIAA Aerospace sciences meeting*, volume 8, pages 5860–5870, Reno, Nevada, 2006.
10. D. Basu, A. Hamed, and K.Das. Assessment of Partially Averaged Navier Stokes (PANS) multiscale model in transonic turbulent separated flows. In *5th Joint ASME/JSME Fluids Engineering Conference*, July 30-August 2, San Diego, California USA, 2007.
11. A. Frendi, A. Tosh, and S. S. Girimaji. Flow past a backward-facing step: Comparison of PANS, DES and URANS results with experiments. *International for Computational Methods in Engineering Science and Mechanics*, 8:23–38, 2007.
12. C.-S. Song and S.-O. Park. Numerical simulation of flow past a square cyclinder using Partially-Averaged Navier-Stokes model. *Journal of Wind Engineering and Industrial Aerodynamics*, 97:37–47, 2009.
13. L. Davidson. Using isotropic synthetic fluctuations as inlet boundary conditions for unsteady simulations. *Advances and Applications in Fluid Mechanics*, 1(1):1–35, 2007.
14. L. Davidson and M. Billson. Hybrid LES-RANS using synthesized turbulent fluctuations for forcing in the interface region. *International Journal of Heat and Fluid Flow*, 27(6):1028–1042, 2006.
15. L. Davidson. Hybrid LES-RANS: back scatter from a scale-similarity model used as forcing. *Phil. Trans. of the Royal Society A*, 367(1899):2905–2915, 2009.
16. L. Davidson. A dissipative scale-similarity model. In *DLES7*, 8–10 September, Trieste, Italy, 2008.
17. C.G. Speziale. Galilean invariance of subgrid-scale stress models in the large-eddy simulation of turbulence. *Journal of Fluid Mechanics*, 156:55–62, 1985.
18. L. Davidson and S.-H. Peng. Hybrid LES-RANS: A one-equation SGS model combined with a $k-\omega$ model for predicting recirculating flows. *International Journal for Numerical Methods in Fluids*, 43:1003–1018, 2003.
19. P. Emvin. *The Full Multigrid Method Applied to Turbulent Flow in Ventilated Enclosures Using Structured and Unstructured Grids*. PhD thesis, Dept. of Thermo and Fluid Dynamics, Chalmers University of Technology, Göteborg, 1997.
20. Alamo and J. Jim. Spectra of the very large anisotropic scales in turbulent channels. *Physics of Fluids*, 15(6):L41–L44, 2003.